Quantum Electronics **50** (2) 197–200 (2020)

LASER APPLICATIONS AND OTHER TOPICS IN QUANTUM ELECTRONICS https://doi.org/10.1070/QEL17141

2D microspatial distribution uniformity of photon detection efficiency and crosstalk probability of multi-pixel photon counters

Lina Liu, Chunling Zhang, Giacomo Gallina, Guoqing Zhang

Abstract. **Two-dimensional (2D) microspatial distribution uniformity of photon detection efficiency (PDE) and optical crosstalk probability P_{ct} of multi-pixel photon counters (MPPCs) is studied. The experimental results show that the 2D spatial distribution of P_{ct} is obviously uneven, i.e. P_{ct} is larger at the corners and edges of a single pixel in MPPCs, which suggest a higher electrical field in the depletion region of the pixel at the corners and edges. The nonuniformity of the 2D spatial distribution of PDE also become evident when the size of the pixels of MPPCs is small, which signifies higher nonuniformity of the electric field distribution in MPPCs with small pixel size. A method is proposed for characterization of the 2D electrical field spatial distribution uniformity in a single pixel of MPPCs, which can be used for guiding the optimisation of the fabrication process of MPPCs and their properties. This promising method can naturally be extended to any Geiger avalanche photodiodes (G-APDs) and their arrays.**

Keywords: *multi-pixel photon counter, silicon photomultiplier, spatial distribution uniformity, photon detection efficiency, optical crosstalk probability, microspatial scale.*

1. Introduction

A silicon photomultiplier (SiPM) [also called a solid-state photomultiplier (SSPM) or a multi-pixel photon counter (MPPC)] has been widely used in many fields, such as nuclear physics [1], medical imaging [2], laser ranging (LIDAR) [3], biophysics [4], quantum optics [5], and quantum informatics [6]. High-quality MPPCs with excellent performance are the basis for their applications. Developing MPPCs with high photon detection efficiency (PDE), low optical crosstalk probability (P_{ct}), low after-pulse probability (P_{ap}) and low dark count rate (DCR) have been an important goal for researchers.

Many efforts have been focused on how to optimise the key parameters of MPPCs [7–10]. For example, the total PDE is enhanced by properly increasing the quantum efficiency (QE), geometric filling factor (GFF) and the avalanche breakdown triggering probability [7, 10]. The total P_{ct} of MPPCs can be reduced by using optical isolation trenches filled with a reflective/absorbing material to confine the photons within the same Geiger avalanche photodiode (G-APD) pixel [8], or by using a buried junction below the active area to prevent diffusion of photon-generated carriers [11] and also by reducing the undepleted region thickness, as well as by using a substrate with very low minority carrier lifetime (short diffusion length) [10]. However, few efforts have been focused on the effects of the two-dimensional (2D) microspatial distribution of the MPPC parameters, such as PDE and P_{ct}, on the actual total value of their counterparts. In a matter of fact, the knowledge of these distributions of some key MPPC parameters are important for guiding the fabrication of relevant devices and optimising the properties.

Unfortunately, there are few works on 2D microspatial mapping of the MPPCs parameters. Ninkovic et al. [12] reported that 2D high electrical field mapping of SiPM can be obtained indirectly by means of infrared photon emission imaging using a high resolution infrared CCD camera, whereas the setup for this method is expensive and the CCD needs to be cooled to low temperature to respond to the IR photons. Eckert et al. [13] did some 2D uniformity scan measurement for some SiPMs in a millimetre scale and found that P_{ct} shows a clear dependence on the geometrical position in SiPM: They attributed this phenomenon to the different number of neighbouring pixels of the SiPM. They also mentioned an additional variation of P_{ct} on a single pixel scale with a 50 and 100 μm pitch, but the reason was not presented. In this paper, the relative 2D PDE maps and 2D P_{ct} maps of the G-APD pixels in micron scale were studied; the results shows that the mechanism for the dependence of PDE and P_{ct} on the geometrical position in SiPM cannot only attributed to the different number of neighbouring G-APD pixels, but also the 2D distribution of the electrical field in the depletion region of single pixel plays an important role on the 2D spatial distribution uniformity of PDE and P_{ct}.

2. Experimental

The schematic of the setup is shown in Fig. 1. A piezoelectric transducer (PZT) nanopositioning system (closed loop resolution, 1 nm; displacement range, 200 μm; PI nanoXYZ, Germany) was employed to control the position of MPPCs. MPPCs (S12571-100C, S12571-025C and S12571-010C, with a pixel size of 100 × 100, 25 × 25 and 10 × 10 μm, respectively; Hamamatsu Photonics K.K., Japan) were fixed in a shielding box and mounted on a nanopositioning stage. A microscope (X-73, Olympus Corp., Japan) was used to focus the laser beam from a picosecond laser source (centre wavelength,

Lina Liu School of Science, Xi'an University of Technology, Xi'an, 710048, China;
Chunling Zhang School of Science, Xi'an University of Architecture and Technology, 710311, China;
Giacomo Gallina TRIUMF, Vancouver, British Columbia V6T 2A3, Canada;
Guoqing Zhang School of Science, Xi'an Polytechnic University, Xi'an, 710048, China; e-mail: zhangg_356@163.com

Received 25 September 2019
Kvantovaya Elektronika **50** (2) 197–200 (2020)
Submitted in English

375 nm; full width at half maximum, 44 ps; repetition rate, 31.125 kHz – 80 MHz; maximum average light power, 0.7 mW; PDL-800D, PicoQuant, Germany) to a tiny spot (about 1 μm in diameter) on the MPPC surface. Note that a pinhole (100 μm in diameter) was used in the optical path of the laser beam between the laser head and the objective to decrease the size of the laser spot. The MPPCs were powered by a programmable power supply; the output avalanche pulses from the MPPC were first amplified by a homemade fast amplifier and then fed to a DPO4102B-L digital phosphor oscilloscope (5 GHz s^{-1}; 1 GHz bandwidth; Tektronix Inc., USA) to observe the waveform and acquire the count rate of the output pulses from the fast amplifier. A PC was used to control the piezo stage controller and acquire the data from the oscilloscope and the nanopositioning system by an LABVIEW program. The 2D map of the avalanche pulse count rate at different photon equivalent (PE) thresholds can be obtained after a 2D sweep by the nanopositioning system.

The intensity of the pulsed laser was weak so that the aver-

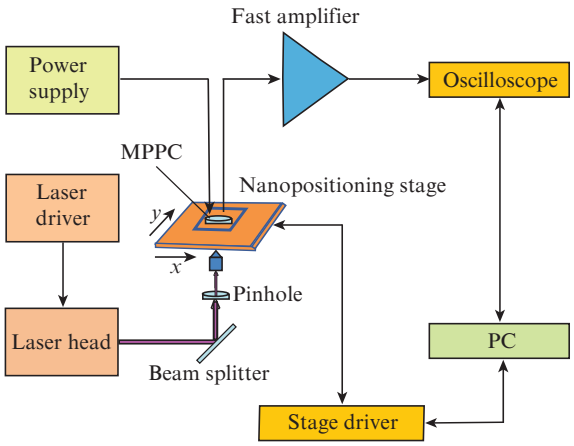

Figure 1. Schematic of the setup for studying the 2D spatial distribution uniformity of PDE and P_{ct}.

age detected photon number is less than 0.1 photon per pulse, which is to make sure that the multi-photon event probability is negligible. To satisfy this condition, we adjusted the intensity of the laser so that the total count rate from the MPPC is less than 10% of the pulse repetition rate $f = 5$ MHz not only to make sure that the pixels of the MPPC can completely recover after previous triggering, but also to ensure that the photon count rate $R_{0.5PE}(x, y)$ is not so low as the background count rate $B_{0.5PE}$ at the PE threshold of 0.5. In this situation, the net count rate (total count rate subtracted by the DCR) of the pulse from the MPPC is a direct reflection of the PDE: The higher the net count rate, the larger the local PDE at the very point in a pixel of the MPPC, which is actually a relative PDE of the MPPC and can be determined as:

$$\eta_{rel}(x, y) = R_{0.5PE}(x, y) - B_{0.5PE}. \quad (1)$$

The $R_{0.5PE}$ can be acquired from the oscilloscope directly, and the $B_{0.5PE}$ can be read after the 2D map data are acquired.

The optical crosstalk probability of the MPPC can be determined as:

$$P_{ct}(x,y) = \frac{R_{1.5PE}(x,y) - P_{1.5PE}}{R_{0.5PE}(x,y) - P_{0.5PE}}. \quad (2)$$

In papers [7, 14] this quantity is referred to as the prompt optical crosstalk probability. In formula (2), $R_{1.5PE}(x, y)$ and $P_{1.5PE}(x, y)$ are the total pulse count rate and the average background count rate measured by setting the threshold level of the oscilloscope at 1.5PE, and $P_{0.5PE}$ is the average photon count rate at the 0.5PE threshold.

3. Results and discussion

Figure 2 shows relative PDE and P_{ct} maps of Hamamatsu MPPCs with different pixel sizes (the background count rates were subtracted) and allows three observations. The first observation is that the 2D spatial configuration of the pixels in MPPCs can be clearly seen in Fig. 2, which is consistent with the visible photographs of the MPPCs (in part) as shown in Fig. 3. The much lower relative PDE and P_{ct} in the gaps between the pixels show a low electrical field in the depletion region of the gaps. It is notable that the components on the photosurface of the MPPCs such as the quenching of the resistors and the metal film obviously block the photons to be absorbed in the high electrical field region, which reduce the effective GFF of the MPPCs and must be taken into account in PDE measurements.

The second observation is that the P_{ct} map in a single pixel is not as uniform as the relative PDE map when the pixel size is no smaller than 25 μm. Figures 2b and 2d clearly show that the P_{ct} is higher at the edge and corner in the pixels and this trends can also be seen indistinctly in Fig. 2f. This phenomenon can be naturally associated with a higher electrical field E at the edge and corner in the pixels. However, there naturally arises an interesting question: If both PDE and P_{ct} are dependent on E, why are the PDE maps more uniform than the P_{ct} maps?

We attribute this fact to a more sensitive dependence of P_{ct} on the E in comparison with PDE. Indeed, on the one hand, it is well known that the dependence of P_{ct} on the applied voltage V is basically superlinear, while the dependence of PDE on V is always sublinear [15, 16], which means that the same increase in V causes a greater increase in P_{ct} than in PDE. The applied voltage can be expressed in the form (the voltage drop from the quenching resistor and the quasi-neutral region can be neglected):

$$V = \int_0^{W(x,y)} \varepsilon(x,y,z)\mathrm{d}z = E(x,y)\,W(x,y), \quad (3)$$

where $W(x, y)$ is the depletion depth (thickness) at a certain point on the surface, $\varepsilon(x, y, z)$ is the local electrical field value at a certain depth z from the top boundary of the depletion region in a p–n junction, and $E(x, y)$ is the integral mean value of the electrical field. Because $W(x, y)$ is proportional to $V^{1/2}$ [17], it is easy to derive a simple relationship, $V \sim E^2$, from Eqn (3). Therefore, a sharper dependence of P_{ct} on the V holds for E. On the other hand, for a given V, the $W(x, y)$ value is smaller at the edge and corner of a pixel because of the smaller curvature of the junction, and thus a higher electrical field E [18]. From the above two points, we can infer that a small increase in E at the edge and corner of the pixels will cause a larger increase in P_{ct}, as compared to PDE. Because E at the edge and corner of the pixels is larger than at

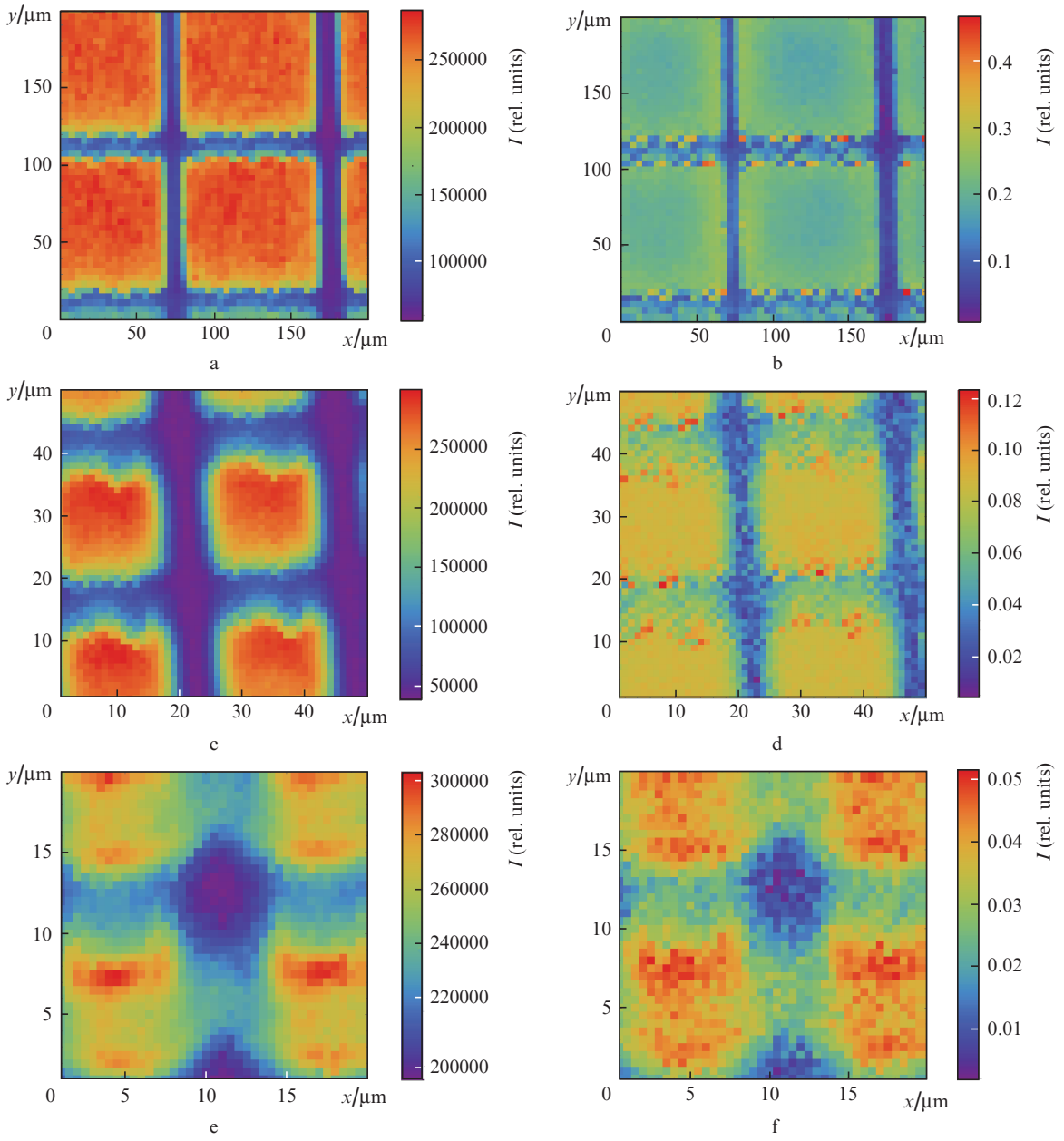

Figure 2. 2D distribution maps of (a, c, e) relative PDE and (c, d, f) optical crosstalk probability P_{ct} of Hamamatsu MPPCs with a pixel size of (a, b) 100 μm (S12571-100C), (c, d) 25 μm (S12571-025C), and (e, f) 10 μm (S12571-010C).

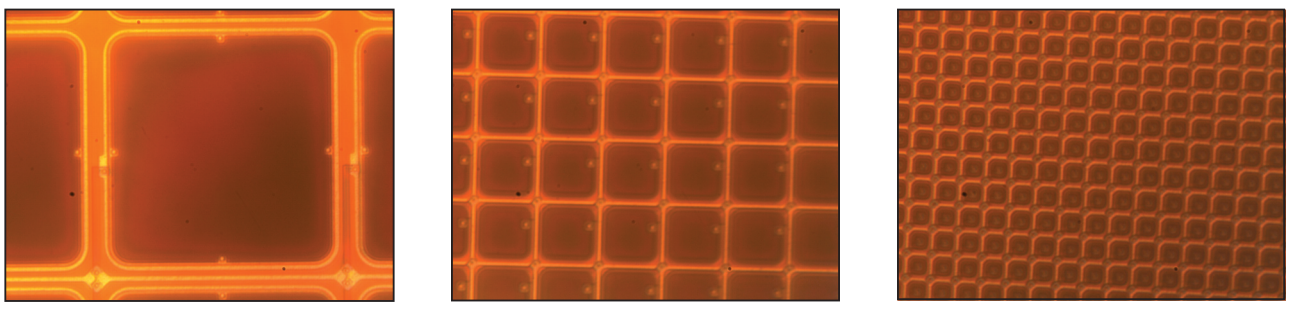

Figure 3. Photographs of the three MPPCs with a pixel size of (a) 100 μm (S12571-100C), (b) 25 μm (S12571-025C), and (c) 10 μm (S12571-010C).

the centre of the pixel, the P_{ct} maps show a clearer nonuniformity than the PDE maps.

The third observation is that the nonuniformity of the 2D spatial distribution of PDE becomes evident when the size of the MPPC pixels is small. This results in a greater nonuniformity of the electric field distribution in the depletion region of the G-APD pixels in MPPCs. However, while MPPCs with a larger pixel size have obviously a larger GFF and thus larger PDE and better PDE uniformity as shown in Figs 2a and 2c, MPPCs with a larger pixel size have larger junction capacitance that enlarges the recovery time and timing performance. Hence, the size of the pixel must be traded off.

From the above, we can assert that some efforts are needed to make the electrical field in the pixels of MPPCs more uniform in order to increase the total PDE and decrease the total P_{ct}, as well as to decrease the total DCR and P_{ap} of SiPMs which have a similar origin and the same mechanism with PDE and P_{ct}. One solution is to make round APD pixels instead of square pixels which are commonly used in most of the existing SiPMs.

4. Conclusions

The two dimensional (2D) microspatial distribution uniformity of the electric field in the depletion region of MPPCs can be revealed by the optical crosstalk probability (P_{ct}) mapping indirectly when the pixel size of the MPPC is relative large, and by both photon detection efficiency and P_{ct} mapping when the pixel size of the MPPC is relative small. The 2D spatial distribution of P_{ct} of MPPCs in a single pixel is obviously uneven, with P_{ct} being larger at the corners and edges of avalanche pixels in MPPCs, which suggests a higher electric field at the corners and edges in the depletion region of the pixels. The nonuniformity of the 2D spatial distribution of PDE also become evident when the size of the pixels of MPPCs is small, which signifies more nonuniformity of the electric field distribution in MPPCs with a small pixel size. Thus, some efforts are required to make the electrical field in the pixel more uniform in order to increase the total PDE and decrease P_{ct} and P_{ap} as well as the dark count rate of MPPCs. In the mean while, we have developed a method for characterising the 2D electrical field spatial distribution uniformity in a single pixel of MPPCs, which can be used for guiding the optimisation of the fabrication process of MPPCs and their properties. Our approaches can naturally be extended to any Geiger avalanche photodiodes and their arrays.

Acknowledgements. This work was supported by the National Natural Science Foundation of China (No. 11975176 and 11705136), Natural Science Basic Research Plan in Shaanxi Province of China (No. 2019JM-139), Special Research Project of Education Department of Shaanxi Province (No. 15JK1443) and National Science Foundation of Shaanxi Province (Grant No. 2018JQ1079).

References

1. Grodzicka-Kobylka M., Moszyński M., Szczęśniak T. *Nuclear Instrum. Methods Phys. Res. Sect. A*, **926**, 129 (2019).
2. Bisogni M.G., Del Guerra A., Belcari N. *Nuclear Instrum. Methods Phys. Res. Sect. A*, **926**, 118 (2019).
3. Acerbi F., Paternoster G., Gola A., Regazzoni V., Zorzi N., Piemonte C. *IEEE J. Quantum Electron.*, **54** (2), 4700107 (2018).
4. Re R., Martinenghi E., Mora A.D., Contini D., Pifferi A., Torricelli A. *Neurophotonics*, **3** (4), 045004 (2016).
5. Chesi G., Malinverno L., Allevi A., et al. *Sci. Rep.*, **9**, 7433 (2019).
6. Balygin K.A., Zaitsev V.I., Klimov A.N., Kulik S.P., Molotkov S.N. *JETP*, **126** (6), 728 (2018) [*Zh. Eksp. Teor. Fiz.*, **153** (6), 879 (2018)].
7. Piemonte C., Gola A. *Nuclear Instrum. Methods Phys. Res. Sect. A*, **926**, 2 (2019).
8. Gola A., Acerbi F., Capasso M. *Sensors*, **19**, 308 (2019).
9. Koyama A., Hamasaki R., Shimazoe K., et al. *Nuclear Instrum. Methods Phys. Res. Sect. A*, **924**, 436 (2019).
10. Acerbi F., Ferri A., Zappala G. *IEEE Trans. Nucl. Sci.*, **62** (3), 1318 (2015).
11. Ghioni M., Cova S., Lacaita A., Ripamonti G. *Electron. Lett.*, **24** (24), 1476 (1988).
12. Ninkovic J., Andricek L., Jendrisyk Ch. *Nuclear Instrum. Methods Phys. Res. Sect. A*, **628** (1), 407 (2011).
13. Eckert P., Schultz-Coulon H.-Ch., et al. *Nuclear Instrum. Methods Phys. Res. Sect. A*, **620**, 217 (2010).
14. Acerbi F., Gundacker S. *Nuclear Instrum. Methods Phys. Res. Sect. A*, **926**, 16 (2019).
15. Gallina G., Giampa P., Retière F., et al. *Nuclear Instrum. Methods Phys. Res. Sect. A*, **940**, 371 (2019).
16. Vacheret A., Barker G.J., Dziewiecki M. *Nuclear Instrum. Methods Phys. Res. Sect. A*, **656**, 69 (2011).
17. Sze S.M., Ng K.K. *Physics of Semiconductor Devices* (Wiley, 2007).
18. Sze S.M., Gibbons G. *Solid-State Electron.*, **9**, 831 (1966).